Robust Monolithic Multiscale Nanoporous Polyimides and Conversion to Isomorphic Carbons

Chakkaravarthy Chidambareswarapattar, Lai Xu, Chariklia Sotiriou-Leventis,* and Nicholas Leventis*

Department of Chemistry, Missouri University of Science and Technology, Rolla, MO 65409, U.S.A. E-mail: leventis@mst.edu; cslevent@mst.edu

Electronic Supplementary Information

		Page No.
Index		S-1
Appendix S.1	Sol formulations and chemical characterization data …..	S-2
Appendix S.2	Small angle x-ray scattering (SAXS) data and data analysis ….	S-11
Appendix S.3	Mechanical characterization under quasi-static compression …	S-13
Appendix S.4	N_2-sorption porosimetry of all **aR-** and both **aL-** materials …..	S-14
Appendix S.5	Hg-intrusion porosimetry of all **aR-** materials ……...	S-16
Appendix S.6	Thermogravimetric analysis (TGA) and solvent uptake ……	S-17
Appendix S.7	Simulated XRD patterns from various optimized structures ….	S-20
Appendix S.8	Characterization data for polyimide-derived carbons (N_2-sorption porosimetry, CHN analysis) …..	S-21

Appendix S.1 Sol formulations and chemical characterization data (CHN analysis, solid state ^{13}C and ^{15}N NMR, FTIR, XRD) of all aerogel samples

Table S.1 Formulations for all sols of this study

sol	PMDA g (mmol) [mL][a]	BTDA g (mmol) [mL][b]	Desmodur RE g [mL][c]	TIPM g (mmol)	N3300A g (mmol) [mL][d]	DMF g (mL)	CH_3CN g (mL)	sol mL	PMDA % w/w [mM]	BTDA % w/w [mM]	TIPM % w/w [mM]	N3300A % w/w [mM]
aR-PMDA-6	3.27 (15) [1.98]		13.59 [13.30]	3.67 (10)		98.8 (104.7)		120.0	2.83 [125]		3.17 [95.5]	
aR-PMDA-12.5	3.27 (15) [1.98]		13.59 [13.30]	3.67 (10)		38.7 (41.0)		56.3	5.89 [266]		6.61 [178]	
aR-PMDA-20	3.27 (15) [1.98]		13.59 [13.30]	3.67 (10)		17.8 (18.9)		34.2	9.43 [439]		10.6 [292]	
aL-PMDA-20	3.27 (15) [1.98]				5.04 (10) [4.34]	24.9 (26.4)	8.31 (10.5)	43.2	7.87 [347]			12.13 [231]
aR-BTDA-6		4.83 (15) [3.07]	13.59 [13.30]	3.67 (10)		123.2 (130.6)		147.0		3.41 [102]	2.59 [68]	
aR-BTDA-12.5		4.83 (15) [3.07]	13.59 [13.30]	3.67 (10)		49.6 (52.5)		68.9		7.10 [218]	5.40 [145]	
aR-BTDA-20		4.83 (15) [3.07]	13.59 [13.30]	3.67 (10)		24.1 (25.5)		41.9		11.4 [358]	8.63 [239]	
aL-BTDA-20		4.83 (15) [3.07]			5.04 (10) [4.34]	29.6 (31.4)	9.87 (12.6)	51.4		8.16 [292]		8.51 [195]

[a] The volume of pyromellitic dianhydride (PMDA) was calculated using its density (1.68 g cm^{-3}).
[b] The volume of benzophenone tetracarboxylic dianhydride (BTDA) was calculated using its density (1.57 g cm^{-3}).
[c] Desmodur RE (Bayer Corporation U.S.A.; density = 1.022 g cm^{-3}) is a 27% w/w solution of TIPM (see Scheme 2 in the main article) in ethyl acetate.
[d] Desmodur N3300A (N3300A) is supplied as a pure compound (viscous liquid, density = 1.17 g cm^{-3}).

Table S.2 CHN Elemental analysis data for **aR-PMDA-xx** and **aR-BTDA-xx** polyimides

material	% C w/w	% H w/w	% N w/w	% residual w/w [a]
aR-PMDA-6	62.80 ± 0.01	3.78 ± 0.01	6.67 ± 0.01	26.75
aR-PMDA-12.5	63.61 ± 0.03	4.01 ± 0.04	6.86 ± 0.01	25.52
aR-PMDA-20	64.11 ± 0.05	4.17 ± 0.02	6.91 ± 0.08	24.81
theoretical for **aR-PMDA-xx** [b]	76.98	3.02	7.92	18.11
aR-BTDA-6	67.70 ± 0.08	3.51 ± 0.04	5.59 ± 0.01	23.20
aR-BTDA-12.5	69.60 ± 0.04	3.41 ± 0.01	5.05 ± 0.04	21.94
aR-BTDA-20	70.15 ± 0.06	3.29 ± 0.06	4.96 ± 0.02	21.6
theoretical for **aR-BTDA-xx** [b]	74.37	3.06	5.84	16.71
2nd generation OH-terminated [c]	69.59	2.99	4.26	
2.66 generation OH-terminated [c]	72.55	3.10	4.61	

[a] By difference, presumably oxygen. [b] Based on the 1.5:1 mol/mol formulation for DANH:TIPM. [c] Assuming hypothetical DANH-terminated hyperbranched structures as in Scheme 2 in the article. Terminal anhydrides are presumed converted to OHs.

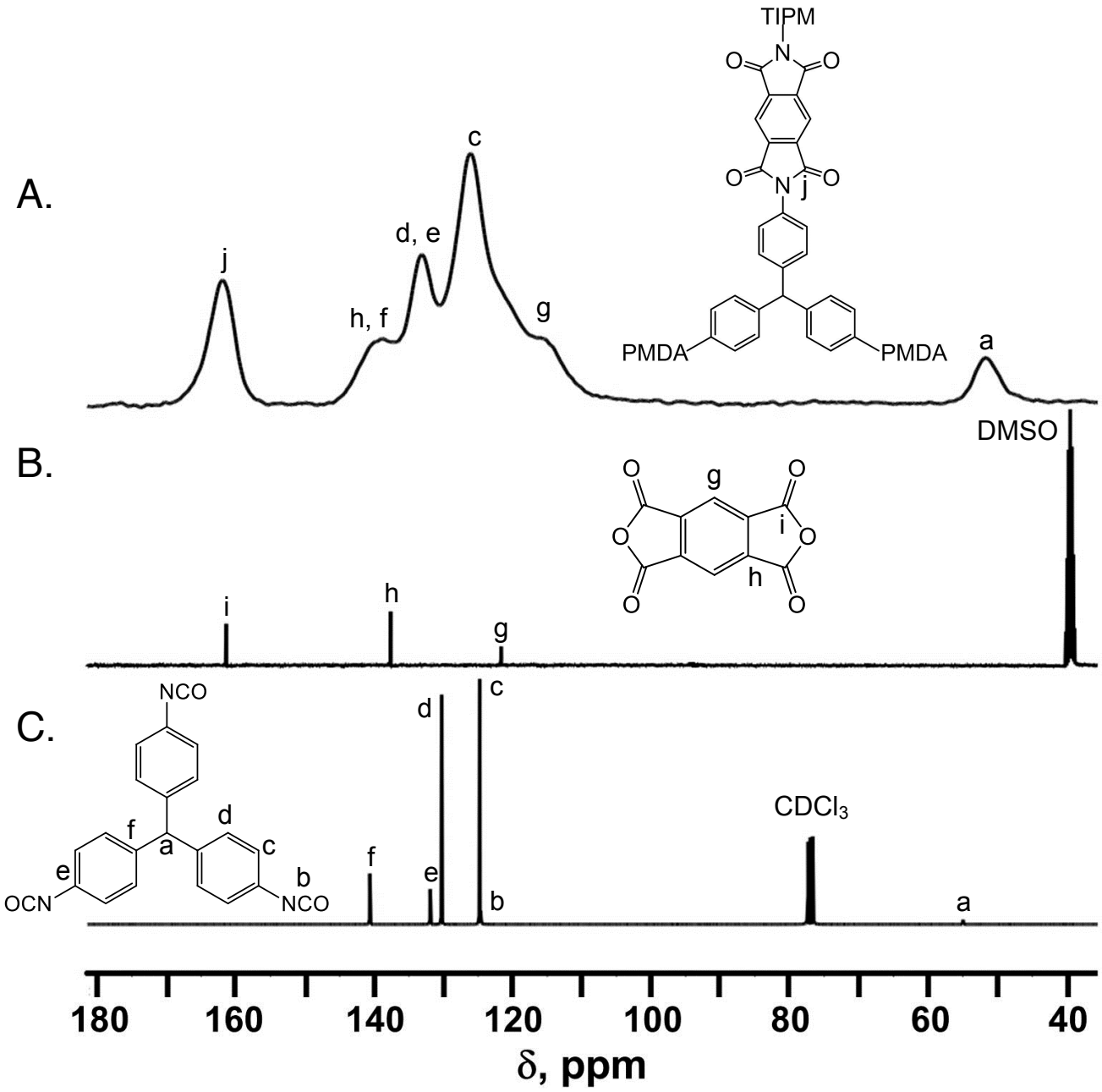

Figure S.1 (A) Solid state CPMAS ^{13}C NMR spectrum of **aR-PMDA-12.5**. (B) Liquid ^{13}C NMR spectrum of PMDA in DMSO-d_6. (C) Liquid ^{13}C NMR spectrum of TIPM in $CDCl_3$.

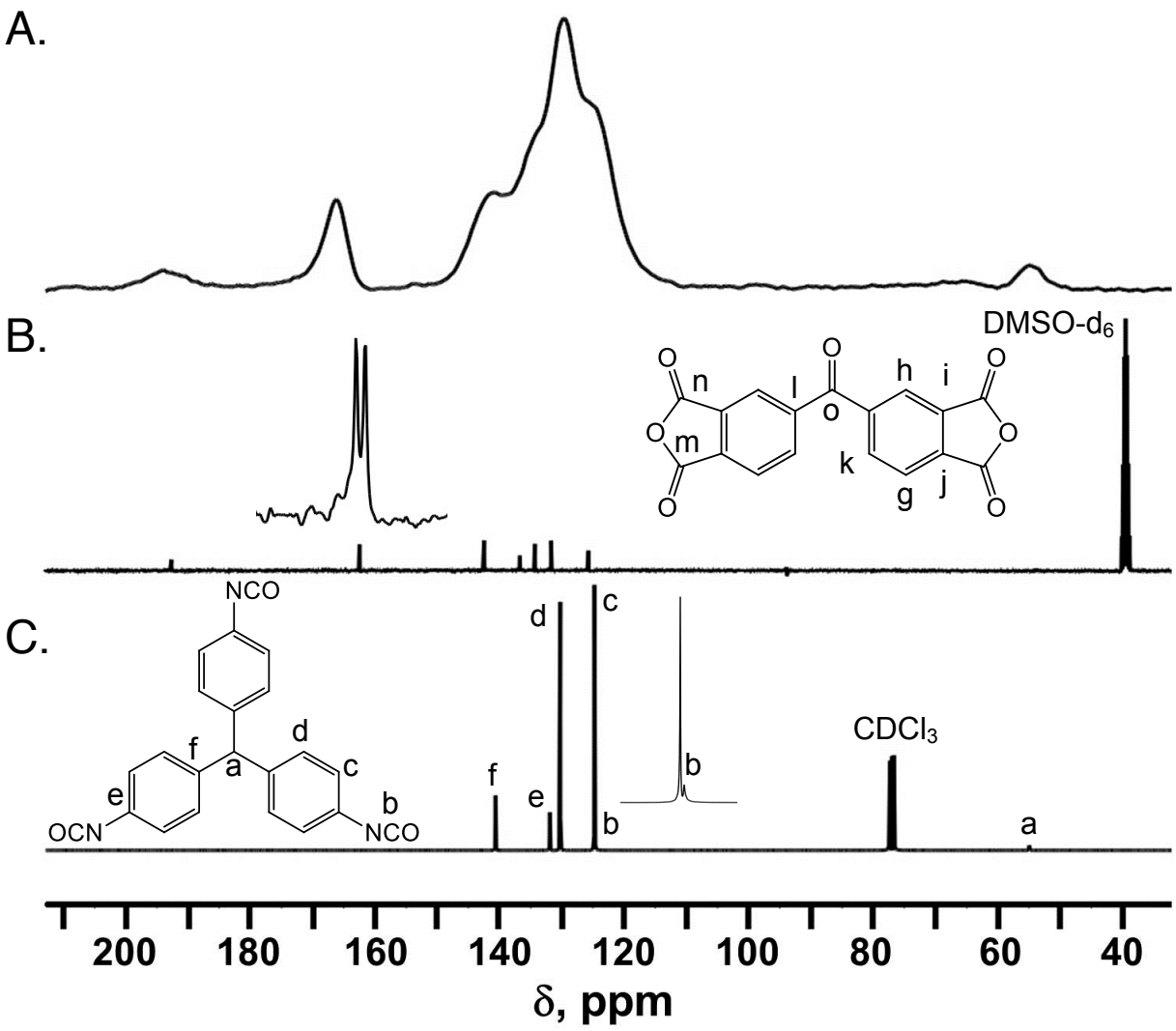

Figure S.2 (A) Solid state CPMAS ^{13}C NMR spectrum of **aR-BTDA-12.5**. (B) Liquid ^{13}C NMR spectrum of BTDA in DMSO-d_6. (C) Liquid ^{13}C NMR spectrum of TIPM in $CDCl_3$.

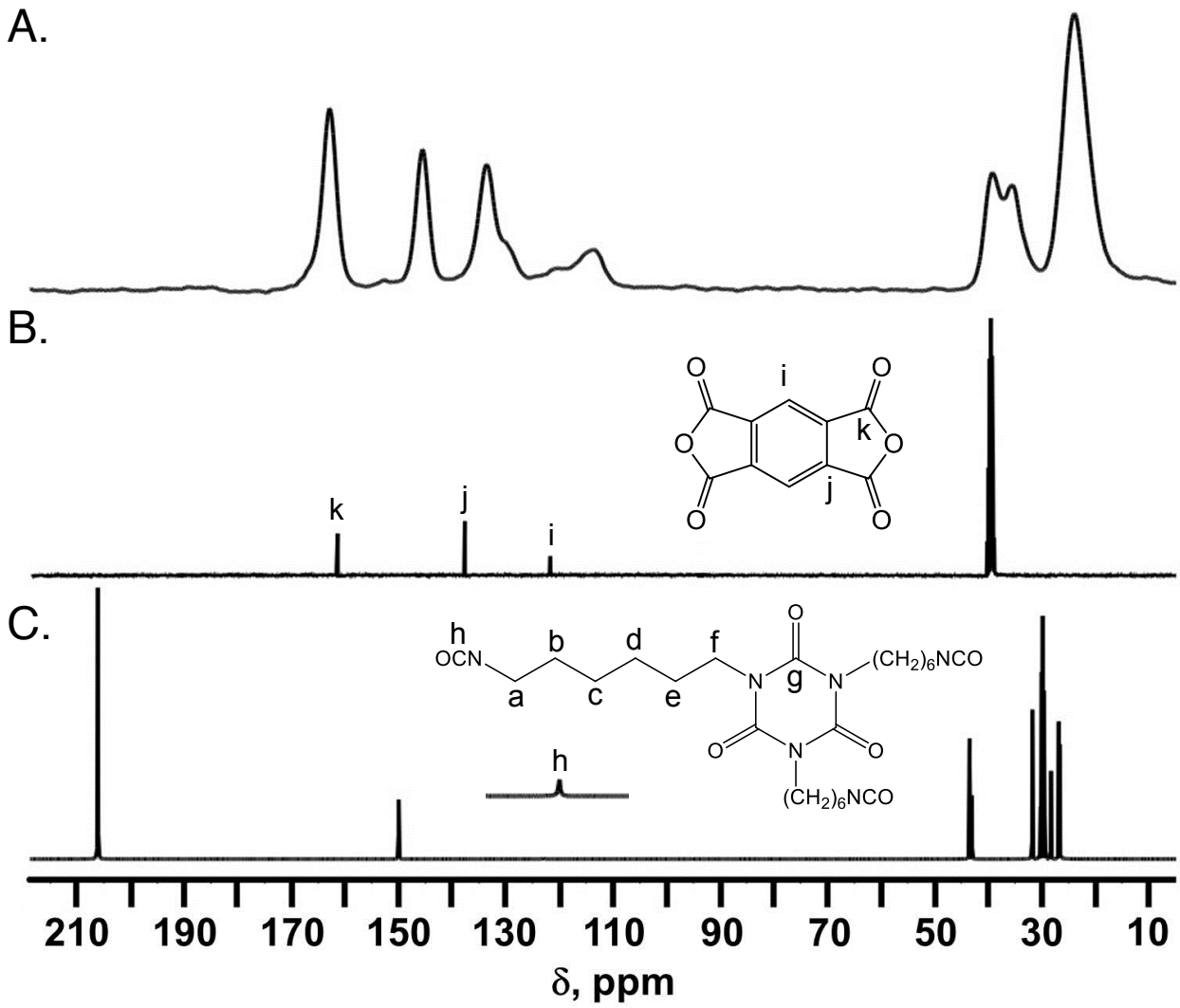

Figure S.3 (A) Solid state CPMAS ^{13}C NMR spectrum of **aL-PMDA-20**. (B) Liquid ^{13}C NMR spectrum of PMDA in DMSO-d_6. (C) Liquid ^{13}C NMR spectrum of N3300A in acetone-d_6.

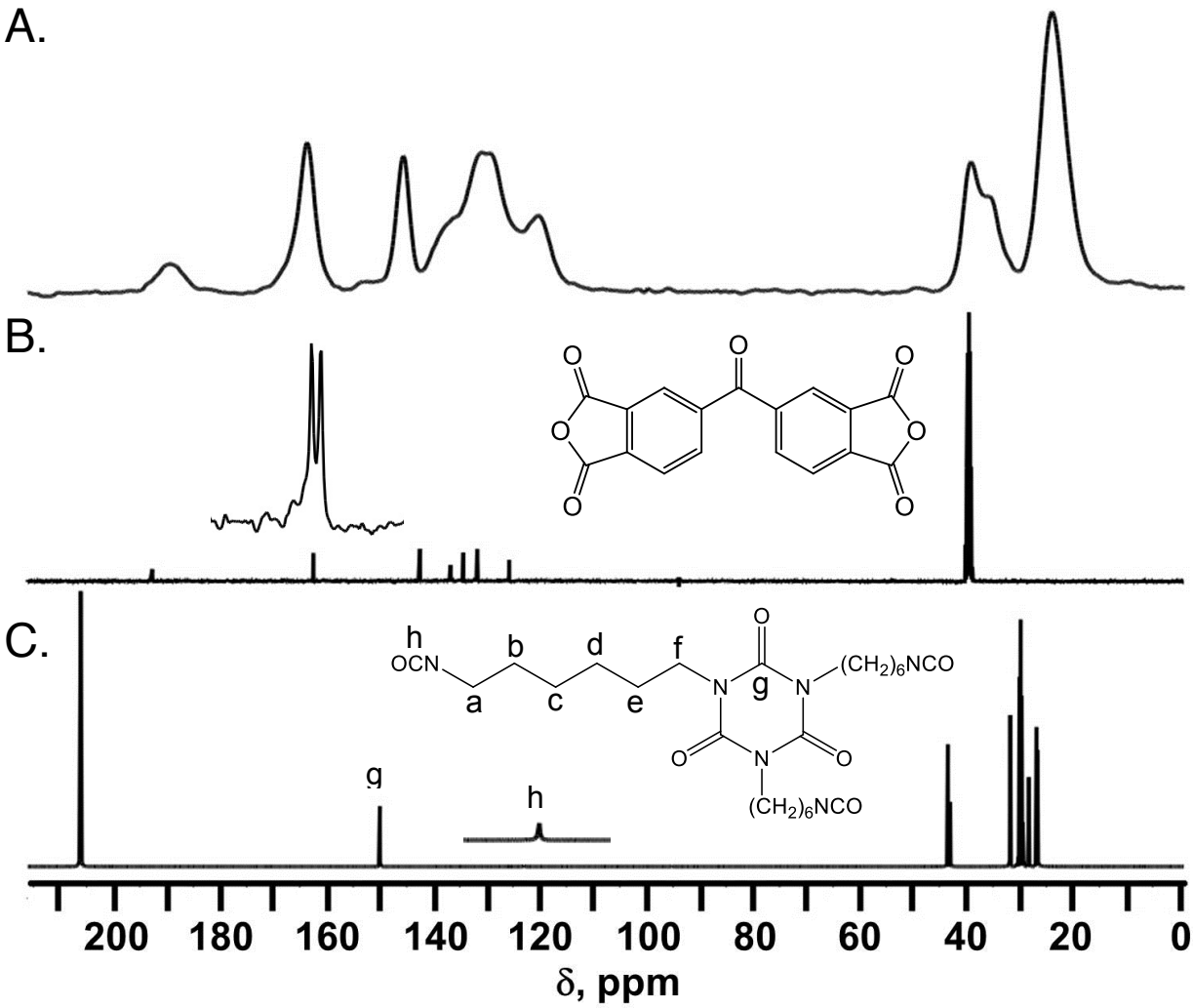

Figure S.4 (A) Solid state CPMAS ^{13}C NMR spectrum of **aL-BTDA-20**. (B) Liquid ^{13}C NMR spectrum of BTDA in DMSO-d_6. (C) Liquid ^{13}C NMR spectrum of N3300A in acetone-d_6.

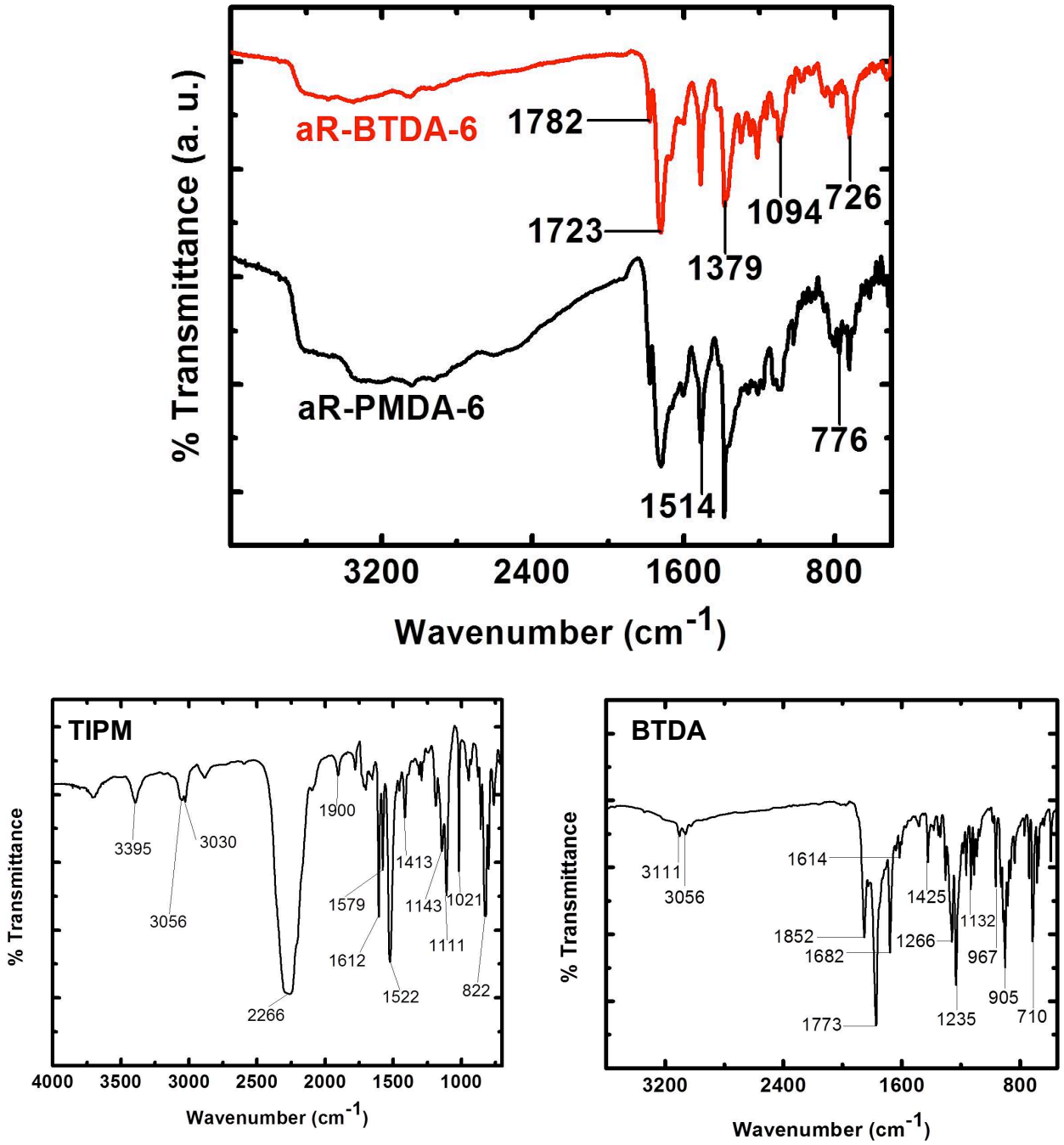

Figure S.5 FTIR spectra of nanoporous polyimides from aromatic TIPM. For comparison the spectra of TIPM and BTDA are shown below. The isocyanate stretch at 2266 cm^{-1} is not present in the spectra of the polyimides. The anhydride bands of BTDA at 1852 cm^{-1} and 1773 cm^{-1} have been replaced by bands at 1782 cm^{-1} and 1723 cm^{-1}, which are assigned to the asymmetric and symmetric stretching vibrations of the imide carbonyls, respectively. The band at ~1379 cm^{-1} is assigned to the C-N-C imide ring stretching. Bands at 1094 cm^{-1} and 776 cm^{-1} are assigned to imide ring bending.

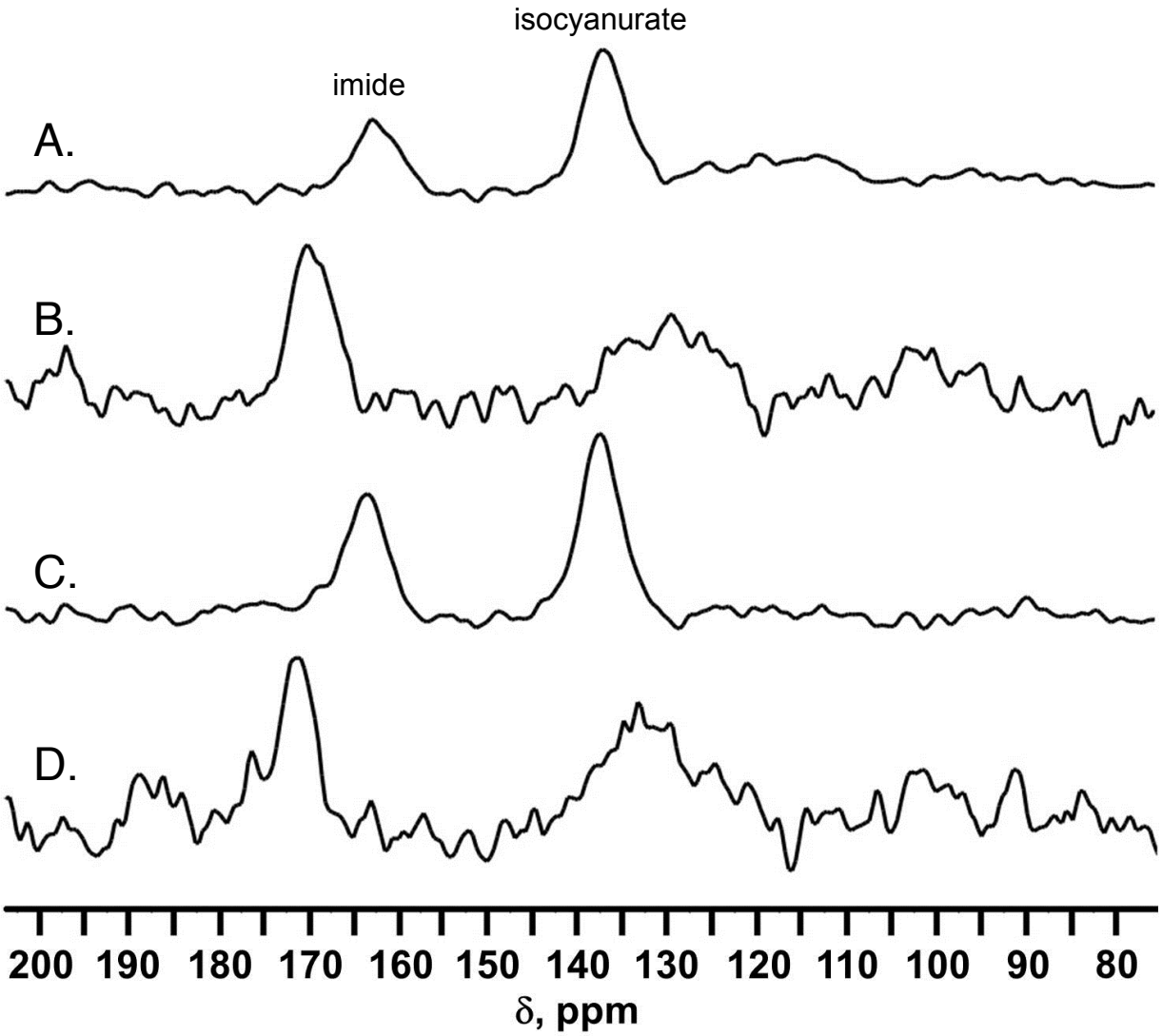

Figure S.6 Solid state CPMAS ^{15}N NMR spectra of nanoporous polyimides, as follows: (A) **aL-BTDA-20**. (B) **aR-BTDA-12.5**. (C) **aL-PMDA-20**. (D) **aR-PMDA-12.5**. Spectra referenced to glycine. For the liquid ^{15}N NMR spectra of the monomers (referenced to CD_3NO_2) see Supporting Information of: N. Leventis, C. Sotiriou-Leventis, N. Chandrasekaran, S. Mulik, Z. J. Larimore, H. Lu, G. Churu, J. T. Mang, *Chem. Mater.* **2010**, *22*, 6692-6710.

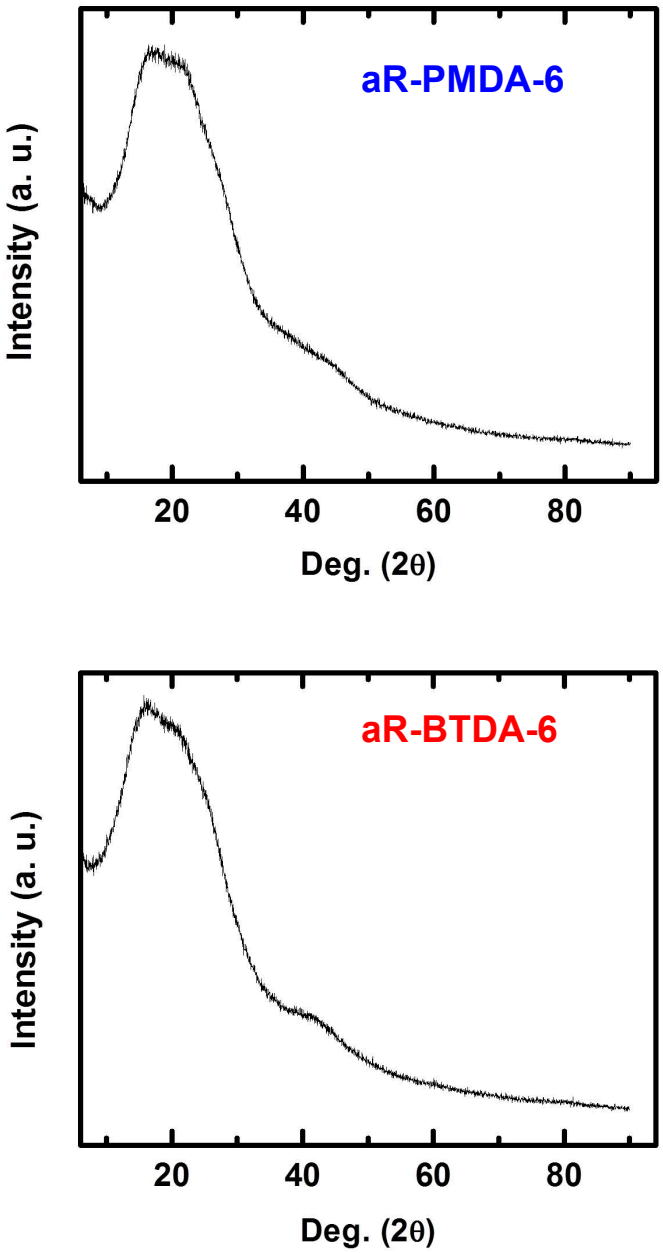

Figure S.7 Representative XRD of nanoporous polyimides derived from aromatic TIPM triisocyanate.

Appendix S.2 Small angle x-ray scattering (SAXS) data and data analysis

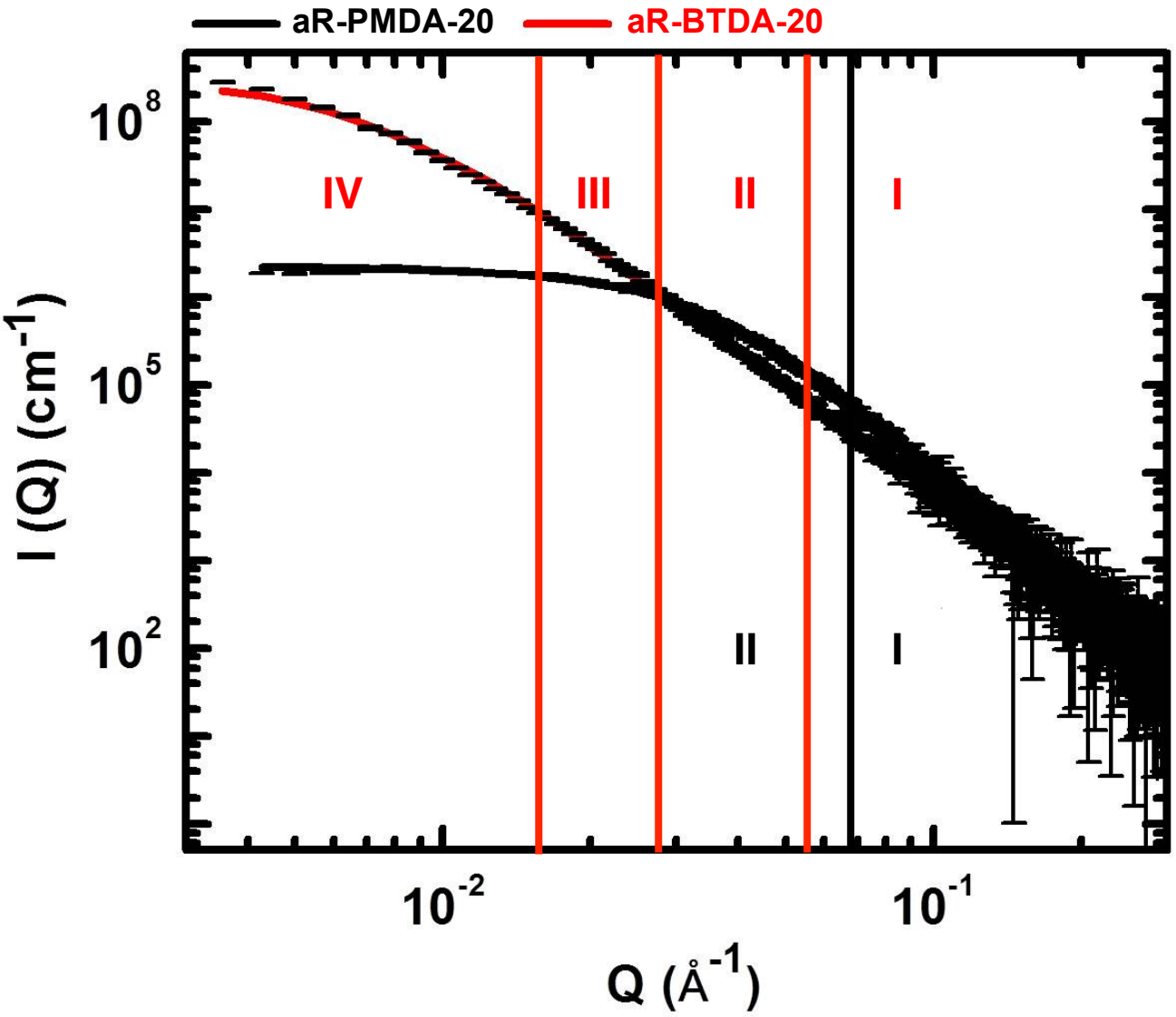

Figure S.8 Typical small angle X-ray scattering (SAXS) data exemplified with **aR-PMDA-20** (information in black) and **aR-BTDA-20** (information in red). Data were fitted to the Beaucage Unified Model. Primary particle radii of gyration (R_G) from first Guinier knee (Region II). Fractal dimension of secondary particles from the slope of power-law Region III. Secondary particle radii of gyration from second Guinier knee (Region IV). Results are summarized in Table S.3.

Table S.3 SAXS characterization data of nanoporous polyimides as indicated

	Primary Particles			Secondary Particles		
bulk density (ρ_b, g cm^{-3})	high-Q slope [a]	$R_G(1)$ [nm] [b]	R_1 [nm] [c]	low-Q slope [d]	$R_G(2)$ [nm] [e]	R_2 [nm] [c]
***aR-PMDA-xx* (-xx: -6; -12.5; -20, respectively)**						
0.437 ± 0.010	-4.00 ± 0.01	13.4 ± 0.1	17.4 ± 0.1	[f]	[f]	[f]
0.684 ± 0.010	-4.00 ± 0.01	6.4 ± 0.1	8.3 ± 0.1	[f]	[f]	[f]
0.715 ± 0.006	-4.00 ± 0.01	5.7 ± 0.1	7.4 ± 0.1	[f]	[f]	[f]
aL-PMDA-20						
0.692 ± 0.017	-4.65 ± 0.01	36.8 ± 0.4	47.8 ± 0.5	[f]	[f]	[f]
***aR-BTDA-xx* (-xx: -6; -12.5; -20, respectively)**						
0.259 ± 0.017	-4.04 ± 0.01	26.6 ± 4.25	34.5 ± 5.5	[f]	[f]	[f]
0.372 ± 0.008	-4.31 ± 0.01	10.4 ± 0.7	13.5 ± 0.9	-2.88 ± 0.48	52.1 ± 7.2	67.7 ± 9.4
0.426 ± 0.007	-4.03 ± 0.16	4.45 ± 0.53	5.8 ± 0.7	-3.87 ± 0.02	32.8 ± 0.6	42.6 ± 0.8
aL-BTDA-20						
0.624 ± 0.027	-4.56 ± 0.01	32.9 ± 0.7	42.7 ± 0.9	[f]	[f]	[f]

Referring to Fig. S.8:

[a] From power-law Region I.

[b] Radii of gyration, $R_G(1)$, from Guinier Region II.

[c] Particle radius $R = R_G/0.77$.

[d] From power-law Region III. For |slope|≤3.0, mass fractal dimension, D_M, of secondary particles: D_M=|slope|. For |slope|>3.0, surface fractal dimension, D_S, of secondary particles: D_S=6-|slope|.

[e] Radii of gyration, $R_G(2)$, from Guinier Region IV.

[f] Beyond the accessible Q-range.

Appendix S.3 Mechanical characterization data under quasi-static compression

Table S.4 Results from mechanical characterization of PI aerogel under uniaxial quasi-static compression at 23 °C

bulk density [ρ_b, g cm^{-3}]	strain rate [s^{-1}]	Young's modulus [*E*, MPa]	speed of sound [m s^{-1}]	yield stress at 2% offset strain [MPa]	ultimate strength [*UCS*, MPa]	ultimate strain [%]	specific energy abs. [*T*, J g^{-1}]
***aR-PMDA-xx* (-xx: -6; -12.5; -20, respectively)**							
0.437 ± 0.010	0.006	143 ± 6	572	4.00 ± 0.00	119 ± 2	76 ± 1	50 ± 2
0.684 ± 0.010	0.006	538 ± 53	887	13.63 ± 0.18	273 ± 6	72 ± 0	82 ± 4
0.715 ± 0.006	0.006	625 ± 35	935	13.16 ± 0.28	298 ± 15	74 ± 1	81 ± 2
aL-PMDA-20							
0.692 ± 0.017	0.008	466 ± 12	820	4.90 ± 0.42	255 ± 18	75 ± 2	47 ± 2
***aR-BTDA-xx* (-xx: -6; -12.5; -20, respectively)**							
0.259 ± 0.017	0.005	44 ± 10	412	0.40 ± 0.08	1.82 ± 0.15	17 ± 2	2.3 ± 0.2
0.372 ± 0.008	0.006	84 ± 1	475	2.75 ± 0.02	112 ± 7	80 ± 1	47 ± 1
0.426 ± 0.007	0.006	140 ± 7	573	3.48 ± 0.38	218 ± 9	82 ± 1	72 ± 2
aL-BTDA-20							
0.624 ± 0.027	0.008	358 ± 38	757	3.95 ± 0.35	297 ± 13	80 ± 0	65 ± 5

Appendix S.4 N_2-sorption porosimetry of all aR- and both aL- materials

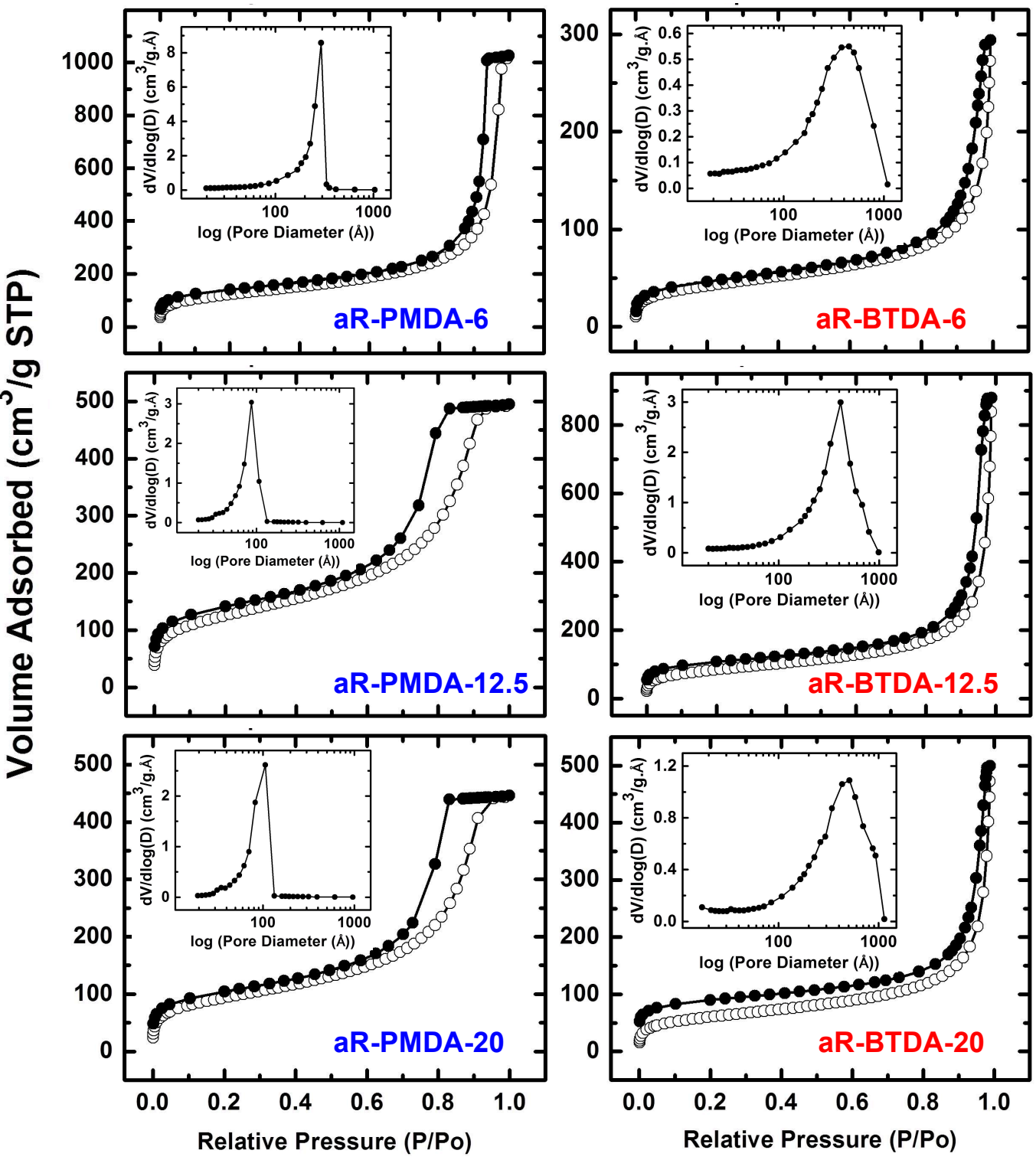

Figure S.9 N_2-sorption isotherms and pore size distributions (Insets) by the BJH method of porous polyimides derived from aromatic TIPM triisocyanate as shown. (Open circles: adsorption; Dark circles: desorption. For results from data analysis see Table 1, main article.)

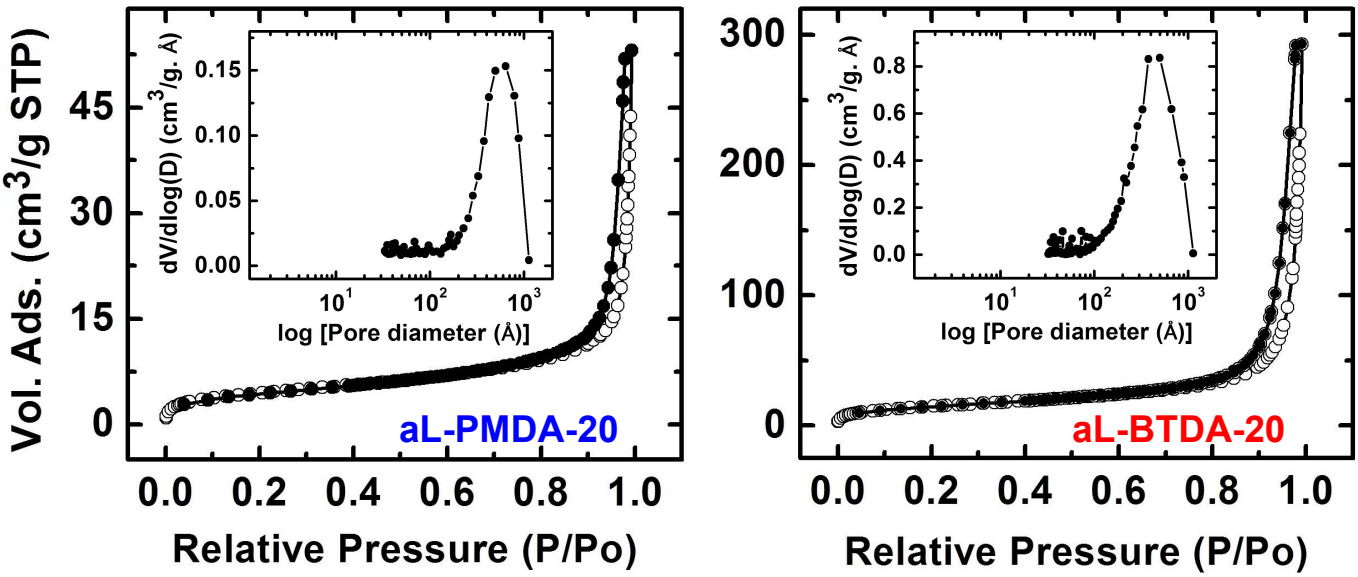

Figure S.10 N_2-sorption isotherms and pore size distributions (Insets) by the BJH method of porous polyimides derived from aliphatic N3300A triisocyanate as shown. (Open circles: adsorption; dark circles: desorption. For results from data analysis see Table 1, main article.

Appendix S.5 Hg-intrusion porosimetry of all aR- materials

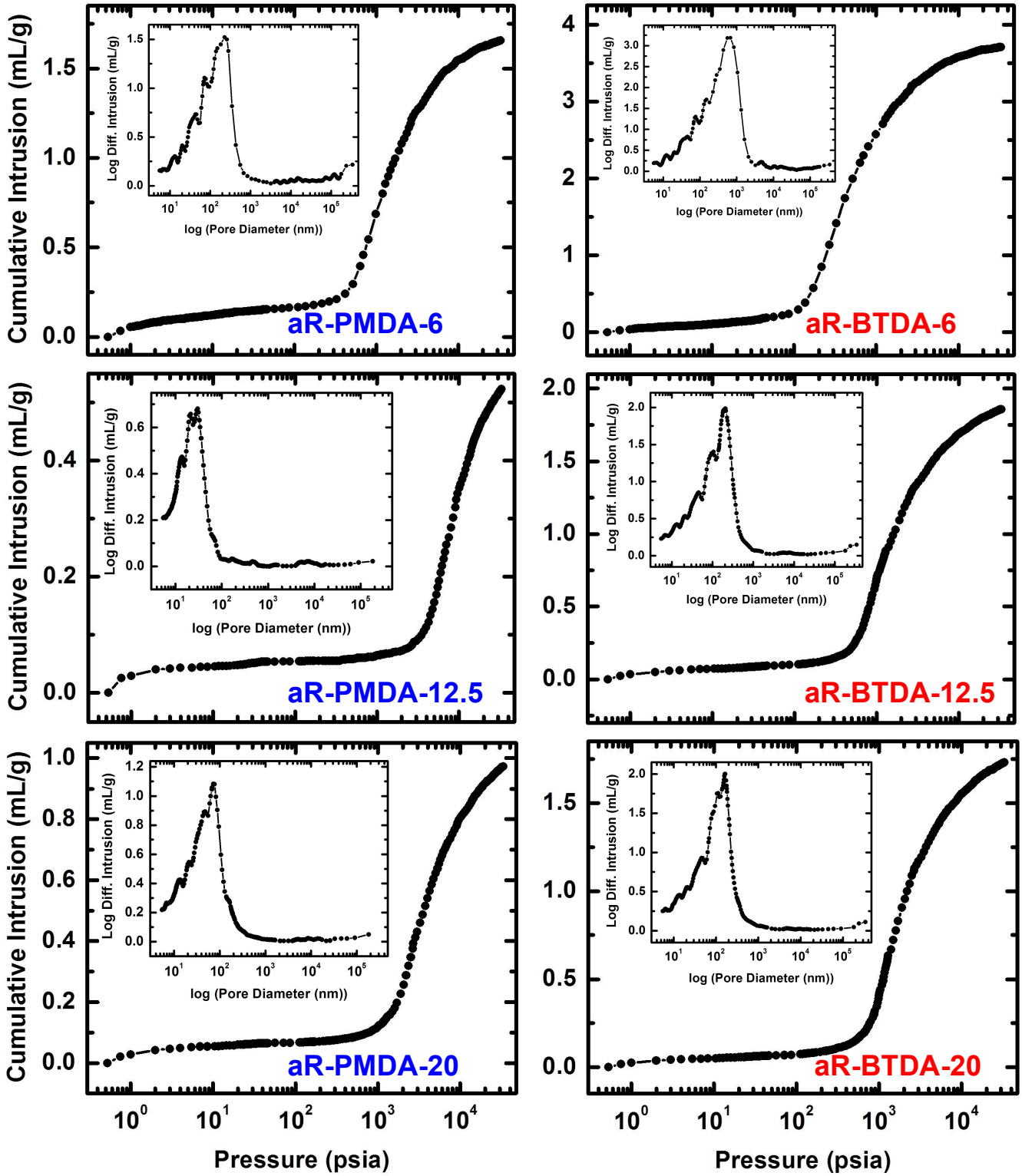

Figure S.11 Hg-intrusion porosimetry of porous polyimides derived from aromatic TIPM triisocyanate as shown. Insets: Pore size distributions. Results in Table 1, main article.

Appendix S.6 Thermogravimetric analysis (TGA) and solvent uptake

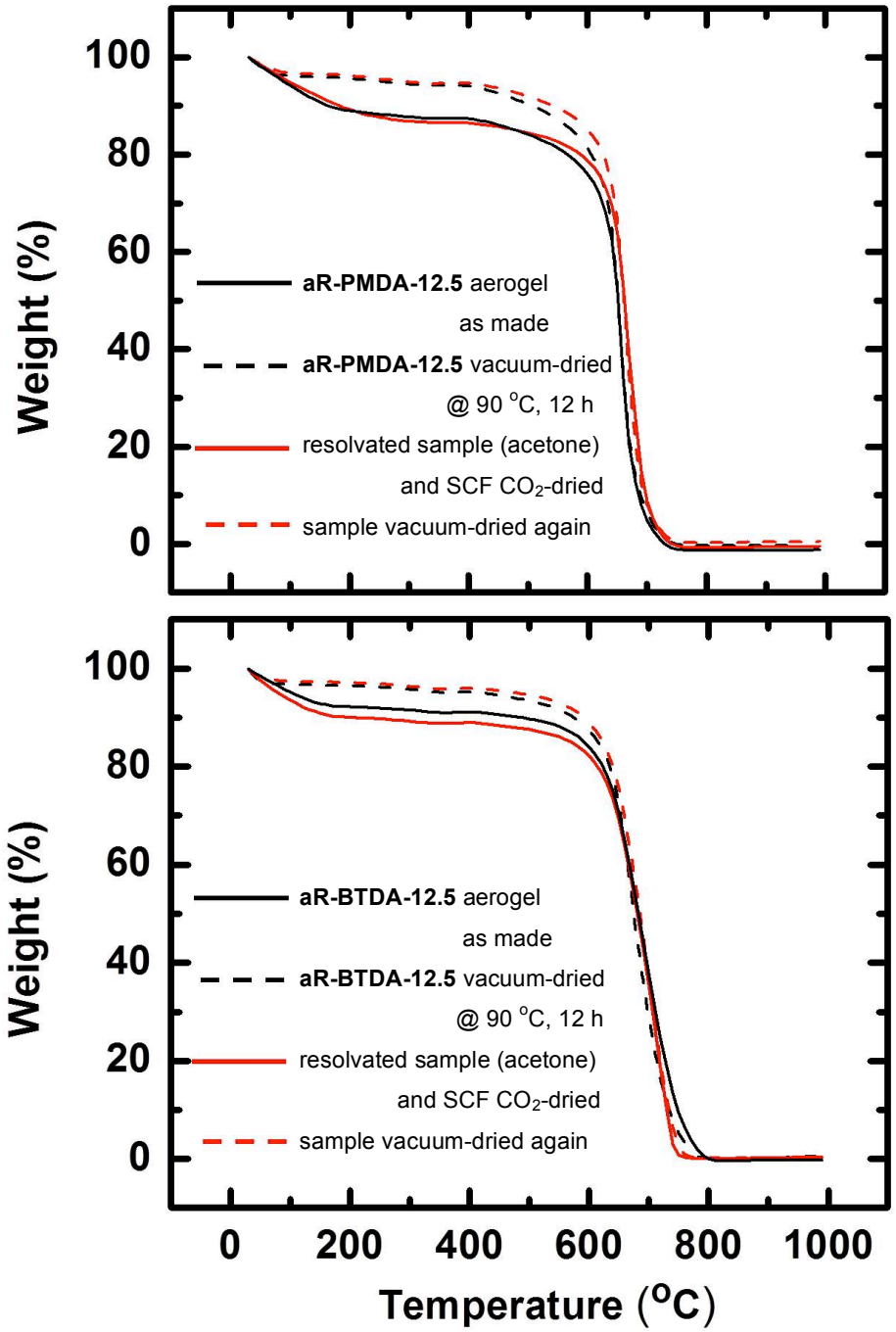

Figure S.12 Thermogravimetric analysis (TGA) in air of the two **aR-DANH-12.5** aerogel samples as indicated. (Heating rate: 10 °C min^{-1}.) The uptake and retention of acetone is not affected by drying via solvent evaporation, hence the pores that retain acetone are not collapsible by surface tension forces suggesting strongly that they are not part of the free volume of the polymer, but rather part of its structure.

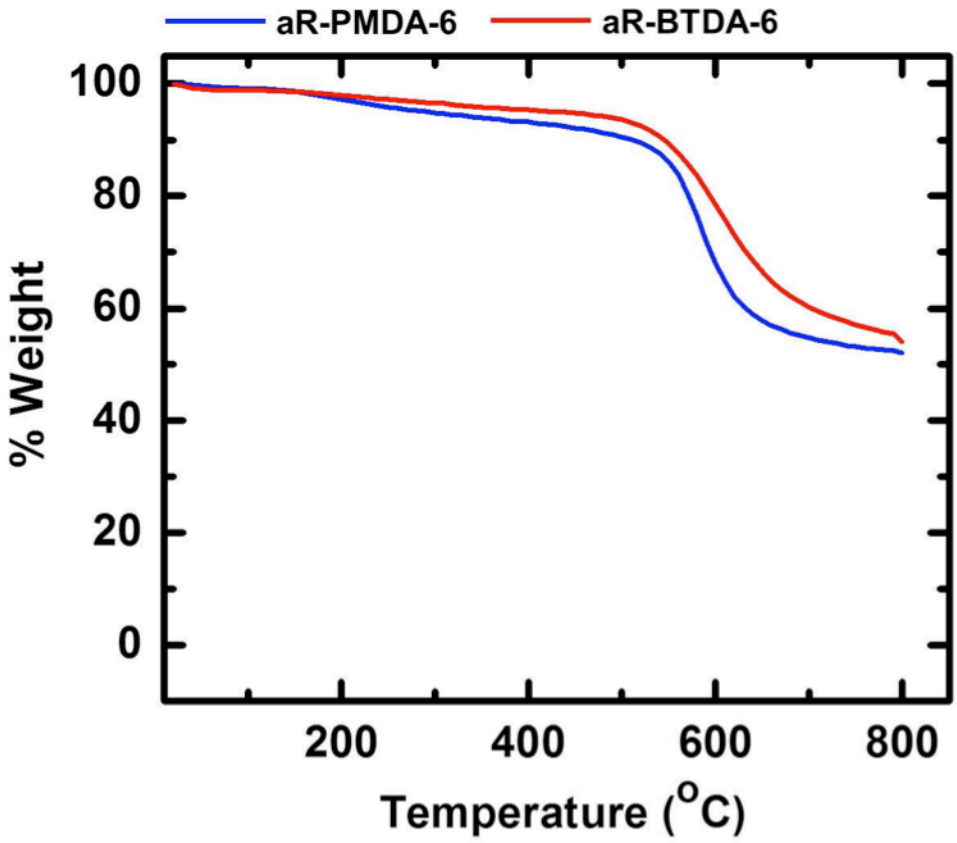

Figure S.13 Thermogravimetric analysis (TGA) under N_2 of the two **aR-DANH-6** samples as indicated. (Heating rate: 10 ^{o}C min^{-1}.)

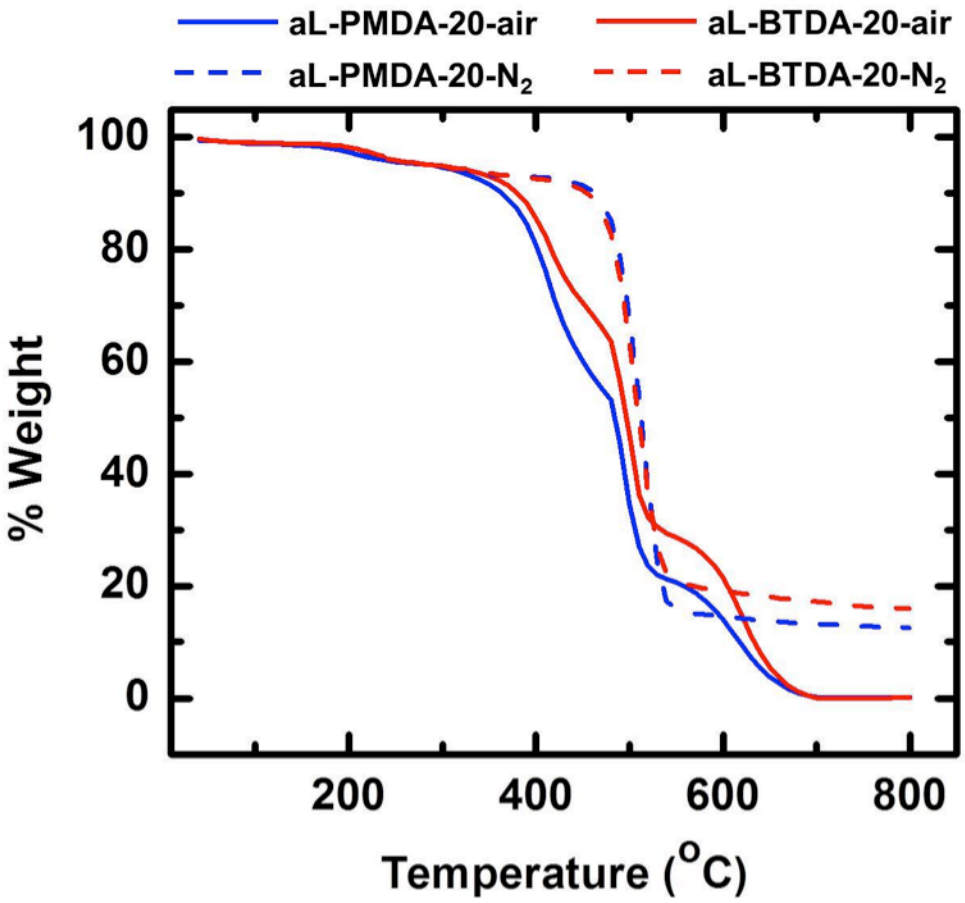

Figure S.14 Thermogravimetric analysis (TGA) under air or N_2 of the two aliphatic triisocyante samples of this study (**aL-DANH-20**) as indicated. (Heating rate: 10 ^{o}C min^{-1}.)

Appendix S.7 Simulated XRD patterns from various optimized structures

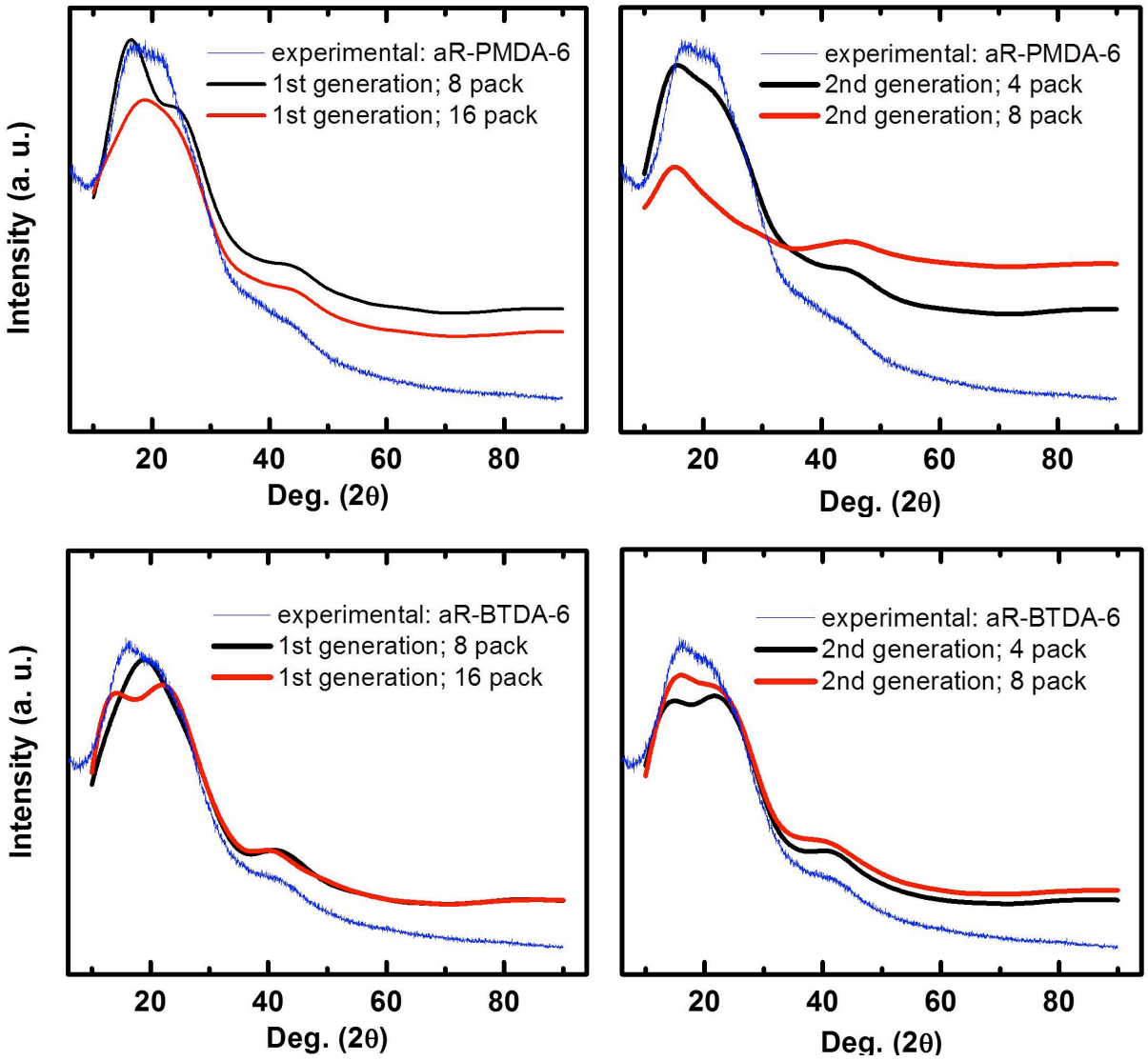

Figure S.15 Simulated versus experimental XRD patterns for **aR-PMDA-xx** and **aR-BTDA-xx** polyimides. "Generation" refers to the hyperbranched growth as shown in Scheme 2 of the main article, and "pack" refers to the number of hyperbrached structures packed in the periodic box and optimized via molecular dynamics relaxation at 298 K for 200 ps.

Appendix S.8 Characterization data for polyimide-derived carbons

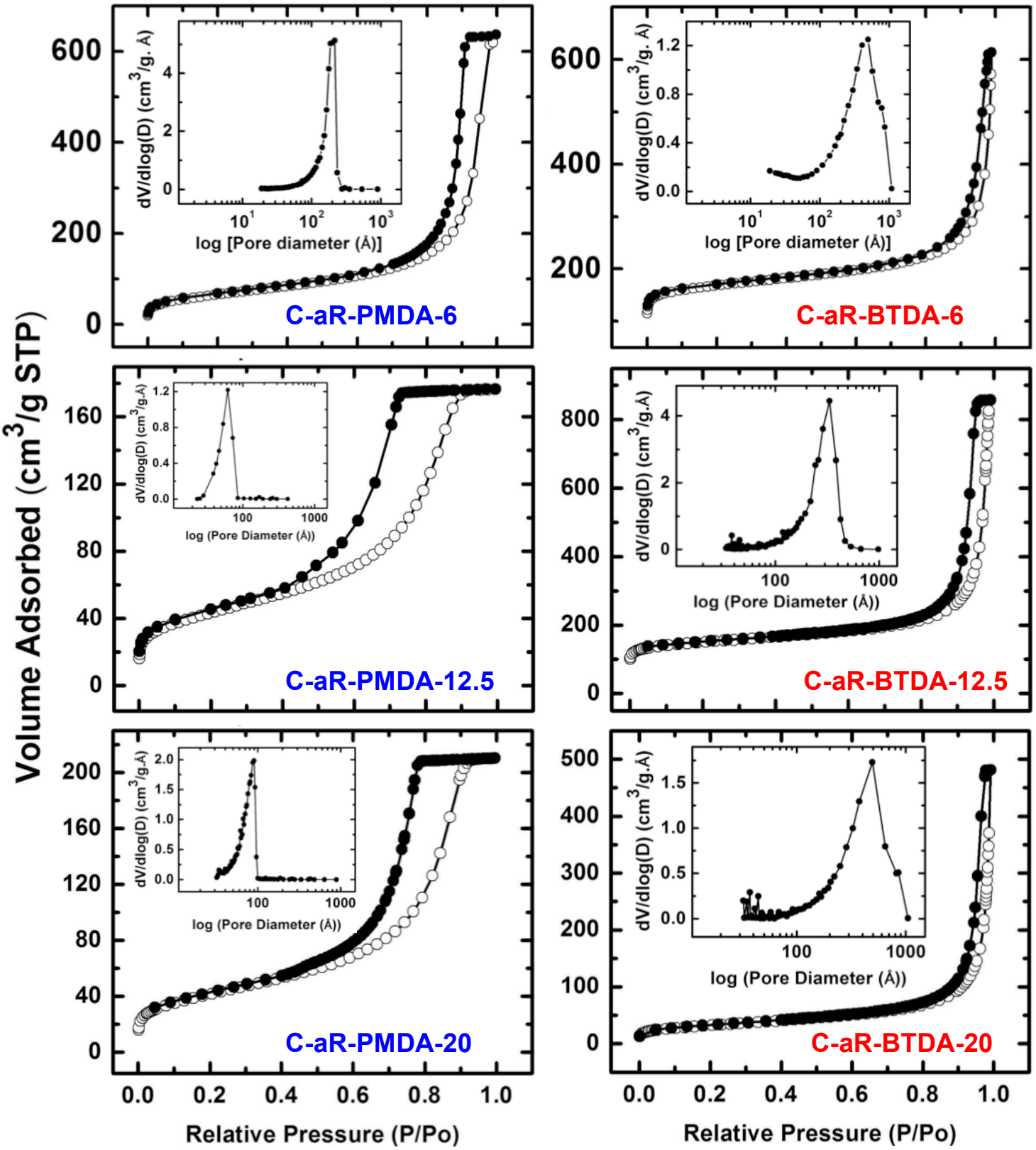

Figure S.16 N_2-Soprtion data of polyimide-derived nanoporous carbons as indicated. Results in Table 2 of main article.

Table S.5 CHN Elemental analysis data for **C-aR-PMDA-xx** and **C-aR-BTDA-xx** carbons

nanoporous carbons	% C w/w	% H w/w	% N w/w	% residual w/w [a]
C-aR-PMDA-6	87.6 ± 0.8	0.41 ± 0.01	7.61 ± 0.2	4.38
C-aR-PMDA-12.5	83.3 ± 0.2	0.38 ± 0.01	10.8 ± 0.6	5.6
C-aR-PMDA-20	81.6 ± 0.08	0.61 ± 0.03	14.8 ± 0.8	2.9
C-aR-BTDA-6	81.8 ± 0.30	0.83 ± 0.01	4.26 ± 0.04	13.11
C-aR-BTDA-12.5	85.4 ± 0.7	0.77 ± 0.03	4.60 ± 0.03	9.23
C-aR-BTDA-20	85.4 ± 0.5	0.5 ± 0.02	5.23 ± 0.18	8.87

[a] By difference, presumably oxygen.